High Power Laser Science and Engineering, (2021), Vol. 9, e19, 8 pages.
doi:10.1017/hpl.2021.4

HIGH POWER LASER SCIENCE AND ENGINEERING

RESEARCH ARTICLE

A novel laser shock post-processing technique on the laser-induced damage resistance of 1ω HfO_2/SiO_2 multilayer coatings

Tangyang Pu[1], Wenwen Liu[1], Yueliang Wang[2], Xiaoming Pan[1], Leiqing Chen[1], and Xiaofeng Liu[3]

[1] *College of Mechanical and Electrical Engineering, Wenzhou University, Wenzhou 325035, China*

[2] *National Engineering Laboratory for Modern Materials Surface Engineering Technology, Institute of New Materials, Guangdong Academy of Sciences, Guangzhou 510651, China*

[3] *Key Laboratory of Materials for High Power Laser, Shanghai Institute of Optics and Fine Mechanics, Shanghai 201800, China*

(Received 12 November 2020; revised 12 January 2021; accepted 19 January 2021)

Abstract

The laser shock processing implemented by a laser-induced high-pressure plasma which propagates into the sample as a shockwave is innovatively applied as a post-processing technique on HfO_2/SiO_2 multilayer coatings for the first time. The pure mechanical post-processing has provided evidence of a considerable promotion effect of the laser-induced damage threshold, which increased by a factor of about 4.6 with appropriate processing parameters. The promotion mechanism is confirmed to be the comprehensive modification of the intrinsic defects and the mechanical properties, which made the applicability of this novel post-processing technique on various types of coatings possible. Based on experiments, an interaction equation for the plasma pressure is established, which clarifies the existence of the critical pressure and provides a theoretical basis for selecting optimal processing parameters. In addition to the further clarification of the underlying damage mechanism, the laser shock post-processing provides a promising technique to realize the comprehensive and effective improvement of the laser-induced damage resistance of coatings.

Keywords: laser-induced damage resistance; laser shock post-processing; multilayer coatings

1. Introduction

As one class of weak damage-resistant components, the optics used in laser applications have always been one of the bottlenecks restricting the development of lasers to high energy and high power. To improve the laser-induced damage resistance of optical coatings, some post-processing techniques have been proposed and researched, such as laser conditioning, which is the current most widely recognized technique and has become a key flux enhancement technique in the construction of the National Ignition Facility. However, the application of laser conditioning is closely related to the coating material[1], coating stack[2], laser wavelength[3], and so on[4,5], based on the promotion mechanism of removing low threshold nodule defects[6,7]. The existing post-processing techniques for coatings mainly have their own application condition and application range, making the discovery of new post-processing techniques that could overcome these limitations pressing and imperative. As a mature and promising surface-treatment technique[8], laser shock processing (LSP) can avoid the direct contact between laser and sample, which has the advantages of no thermal effect, good adaptability, and significant strengthening[9]. LSP has been widely and successfully applied in improving the fatigue durability[10,11], corrosion[12], wear resistance[13], and other mechanical properties of metals and alloys[14,15]. Inspired by the cold processing and high-pressure characteristics of LSP, researchers have attempted to apply LSP in the field of optics in recent years. Millot *et al.*[16] and Shen*et al.*[17] reported laser-driven shock experiments on fused silica to find its melting temperature at 500 GPa and the phase transformation process, respectively.

In this paper, we innovatively applied an LSP technique as a post-processing technology of the porous HfO_2/SiO_2

Correspondence to: W. W. Liu, College of Mechanical and Electrical Engineering, Wenzhou University, Wenzhou 325035, China. Email: sophialww@163.com

multilayer coatings deposited by electron beam evaporation for the first time. We hoped that a comprehensive modification of intrinsic defects, mechanical properties, compactness, and so on can be achieved, because the laser shock post-processing (LSPP) is a pure mechanical process implemented by the laser-induced high-pressure plasma that propagates into the sample as a shockwave[18]. The effects of LSPP with different processing parameters on the laser damage behaviors of dielectric coatings were analyzed, including the damage morphologies, damage precursors, and microproperties. In addition, a modified equation of the total pressure in LSPP process was established to provide a theoretical basis for selecting optimal LSPP parameters and clarify the underlying modification mechanism further.

2. Materials and methods

2.1. Sample preparation

The HfO_2/SiO_2 highly reflective (HR) coatings with thickness of 6 μm were deposited on K9 substrate with a diameter of 50 mm. All coatings used in this study were deposited in the same coating chamber by electron beam evaporation. When the incident angle was 45°, the reflectance at 1064 nm was greater than 99.5%, which was not weakened for coatings that had undergone LSPP of parameters discussed here.

2.2. Experimental setup for LSPP and one-on-one damage test

As in the apparatus shown schematically in Figure 1(a), the LSPP experiments were performed using a *Q*-switched Nd:YAG laser operating at 1 Hz repetition rate with a wavelength of 1064 nm and a pulse width of 8 ns. The laser energies varied within the range of 0.2–2 J with a minimum interval of 0.1 J and a spot diameter of 2 mm. The black paint coating with a thickness of ~0.1 mm was used as an absorbing layer to absorb the irradiated laser energy and form plasma, which protected the sample surface from thermal effect. A water layer with a thickness of about 1–2 mm was used as the transparent confining layer to trap the expanding plasma and create a high-pressure shockwave. Raster scanning with overlapping rates of 30% and 50% was performed on the treated area of 30 mm× 18 mm. To prevent macro-damage or degrade the original performance, the maximum allowable laser energies of the two overlapping rates were separately verified to be 0.6 and 0.4 J. The number of scans was one unless noted otherwise. After the LSPP, the excess water and residual black paint remaining on the sample were removed using dust-free cloth and acetone. Then, a combination of high-pressure spray rinsing and ultrasonic cleaning was performed to get a full range of thorough cleaning. The laser damage test apparatus is shown in Figure 1(b), in which a Nd:YAG laser operating at 5 Hz repetition rate with a wavelength of 1064 nm and a pulse width of 12 ns was used. An energy attenuator, composed of a half-wave plate and a polarizer, was employed to adjust the pulse energy and the polarization state. When the incident angle was 45° (S-polarized), the equivalent area of the spot was about 0.99 mm^2. The specific test procedure and error analysis in one-on-one mode can be found in Ref. [19].

2.3. Analysis method

The microstructures and microcharacteristics of HR coatings were characterized by X-ray diffraction (XRD; Bruker D8 ADVANCE). The details of the damage morphologies and inner structures were obtained using a focused ion beam (FIB; Helios-G4-CX, Thermo Scientific) with the functions of a scanning electron microscope.

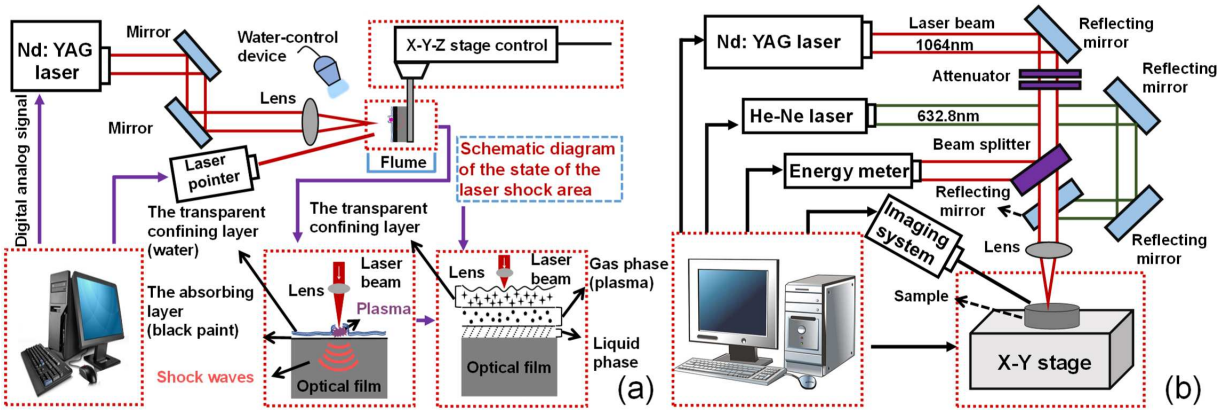

Figure 1. Experimental schematic of (a) LSPP and (b) one-on-one damage test.

https://doi.org/10.1017/hpl.2021.4 Published online by Cambridge University Press

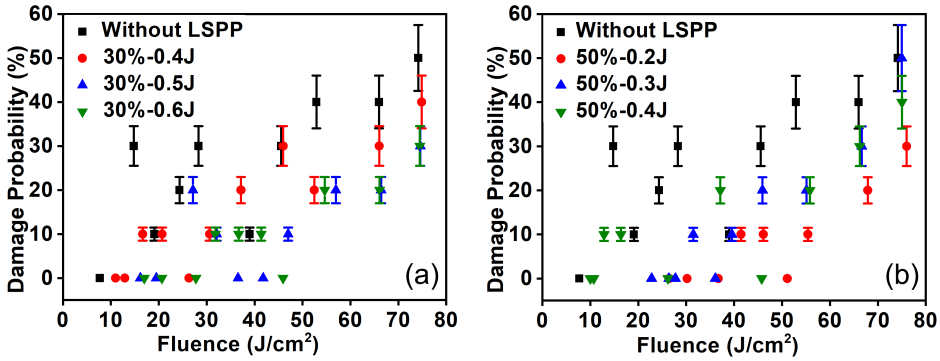

Figure 2. The one-on-one damage probabilities of coatings without and with LSPP at overlapping rates of (a) 30% and (b) 50%.

3. Results and discussion

3.1. Experimental results

The damage probabilities of HR coatings without and with LSPP are shown in Figure 2, which evidently showed a decrease in damage probability and an increase in damage threshold for coatings that had undergone LSPP with appropriate process parameters. When the overlapping rate was 30%, as shown in Figure 2(a), the laser-induced damage resistance of HR coatings was increasingly enhanced with processed laser energy which varied from 0.4 to 0.6 J. When the laser energy was at the maximum 0.6 J, the laser-induced damage threshold (LIDT) had increased to 27.8 J/cm^2 and the maximum damage probability decreased to only 30% at 74.9 J/cm^2. When the overlapping rate was improved to 50% as shown in Figure 2(b), although the laser-induced damage resistance had always been improved as the processed laser energy in the range of 0.2–0.4 J, the LIDT and the damage probability began to decrease and increase with laser energy, respectively. When the laser energy was of the minimum 0.2 J, the LIDT had achieved the maximum value of 36.7 J/cm^2, and the maximum damage probability also decreased to about 30% at 76.5 J/cm^2. Compared with the coatings without LSPP which had a low LIDT of 8 J/cm^2, the reason for the enhancement of laser damage resistance after LSPP was possibly because of the comprehensive modification of the intrinsic defects and the mechanical properties which made defects less susceptible to excitation.

3.2. Microstructures and microcharacteristics

As the XRD pattern shown in Figures 3(a) and 3(b), though no new phase was generated after LSPP, the peaks were broadened and shifted (such as the example of the (020) peak shown in Figures 3(c) and 3(d)). According to the full width at half maximum (FWHM) and diffraction angle obtained by fitting of XRD line profiles with the Pearson VII function[20], the microstress was acquired by the Williamson–Hall plots method[21–23], as shown in Figure 4. The microstress in the figure was negative, indicating that the stress direction was perpendicular to the surface and downward, which illustrated that the existing microstress was in the form of compressive stress. As the inherent stress in the coatings was very small and tended towards zero, the microstress herein could be considered as the value of the residual stress. It was clear the residual stress of coatings with LSPP of reasonable parameters exhibited considerable increment, as shown by the dotted line in Figure 4, which indicated the enhancement of mechanical properties such as bonding force between interfaces. The microstress soon reached an extreme value which basically remained unchanged as the shock energy or overlapping rate increased further, and thus the LIDT was mainly affected by defects at this time. The LIDTs manifested an increasing trend until a maximum value at an overlapping rate of 50% with laser energy of 0.2 J first and then a decreasing trend as laser energy continued to increase. When the laser energy was 0.4 J with an overlapping rate of 50%, the LIDT had decreased to 10.7 J/cm^2, which was similar to that of coatings without LSPP. The different variation trends between microstress and LIDT indicated defects had a major role in affecting the laser-induced damage resistance of coatings, compared with mechanical properties. However, the enhancement of the mechanical properties could also decrease the probability of defect excitement and improve the laser-induced damage resistance, which requires further study in the future to confirm. In addition, the fact that the LIDT also had low values with high microstress in some cases indicated that the excessive laser energy used in the LSPP process may have no positive effect or possibly a negative effect on defects. Compared with the existing post-processing techniques, LSPP has been found to have a comprehensive modification of intrinsic defects and mechanical properties, which may overcome the limitations of the current techniques on improving the laser-induced damage resistance of coatings. Beyond that, the benefit of LSPP on the packing density and water absorption of the porous HR coatings, as well as the applications on various coatings, will be systematically studied in future work.

https://doi.org/10.1017/hpl.2021.4 Published online by Cambridge University Press

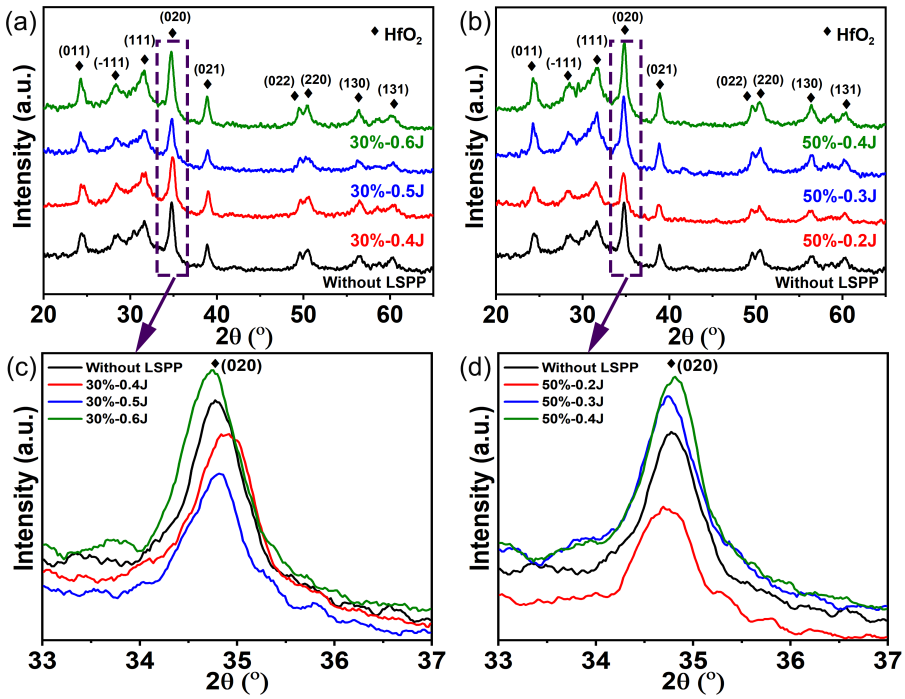

Figure 3. XRD patterns of coatings with LSPP at overlapping rate of (a) 30% and (b) 50%, with (c) and (d) showing the corresponding specific XRD patterns of the (020) peak.

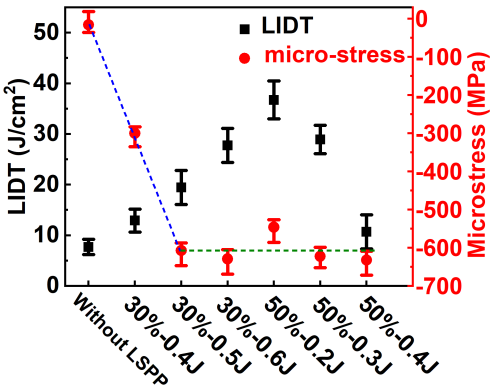

Figure 4. Statistical chart of the microstress and LIDT.

3.3. Morphology and depth of damage sites

Since the laser-induced damage resistance of coatings was affected by the combined effects of mechanical properties and damage defects, damage morphologies and depth characteristics of 1064 nm HR coatings with and without LSPP were studied to discover and clarify the process and effect of LSPP on the damage precursors. It was found that there were two typical damage morphologies[19]: large-area plasma scald without damage pits in the center (marked as type I) as shown in Figure 5(a); and large-area plasma scald with micrometer-sized pits in the center (marked as type II) as shown in Figure 5(e). It is well known that damages of coatings are induced by defects in nanosecond-pulse regime. As the inset shown in Figure 5(a), because no pits are observed at the original position of the plasma scald under scanning electron microscopy (SEM) at a higher magnification but a maximum depth of about dozens of nanometers, the most likely precursors for damage morphology of type I are assumed to be the submicrometer-sized defects distributed within the outermost layer, making the actual existing pits of too small size be observable. An analysis of the morphology of damage sites (Figures 5(b)–5(d)) and the corresponding FIB cross-sections (Figures 5(f)–5(h)) for coatings with or without LSPP found the bottoms of the micrometer-sized pits, namely the locations of the precursors, were randomly distributed at the relatively shallow interfaces, but always at or below the sixth interface which was of relatively high electric-field intensity[19].

The size distributions of the surrounding plasma scald of coatings with and without LSPP are depicted in Figure 6. As the laser irradiated at an oblique angle of 45°, the shape of the scalding was elliptical[24], the size or diameter of which was defined as its major axis. For a single coating without or with LSPP of same processing parameters, the scald diameter increased almost linearly with the incident laser fluence from 100 μm or so to about 1 mm, while varying by hundreds of micrometers at one laser fluence. It was found that LSPP almost had no effect on the size distribution of scalds which were mainly determined by the properties of damage precursors.

Although the LSPP process looked as if it had almost no influence on the damage morphology and damage depth, the individual minimum laser fluences to induce damage

https://doi.org/10.1017/hpl.2021.4 Published online by Cambridge University Press

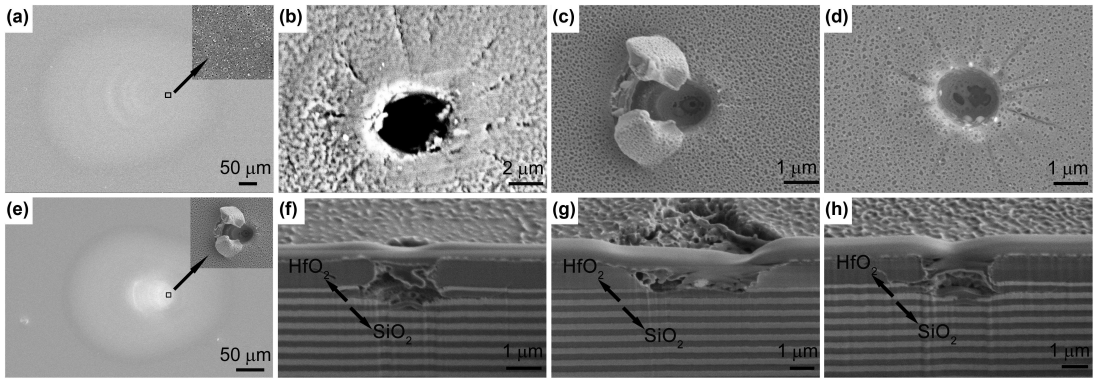

Figure 5. The two typical damage morphologies of coatings with LSPP processed by an energy of 0.6 J at overlapping rate of 30% tested by SEM at (a) 31.8 J/cm^2 and (e) 74.9 J/cm^2, respectively. SEM and FIB images of the central pits of coatings: (b) and (f) without LSPP damaged at 74.1 J/cm^2; (c) and (g) with LSPP processed by energy of 0.6 J at overlapping rate of 30%, and damaged at 74.9 J/cm^2; (d) and (h) with LSPP processed by energy of 0.2 J at overlapping rate of 50%, and damaged at 76.5 J/cm^2.

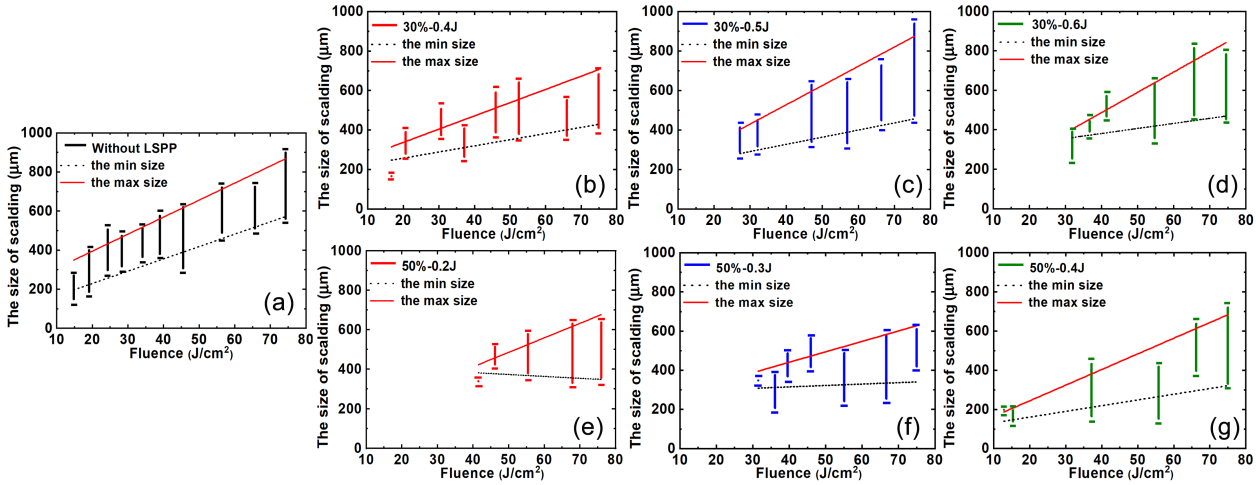

Figure 6. Size distribution of plasma scalds versus laser fluence of coatings: (a) without LSPP; (b)–(d) processed at an overlapping rate of 30%; (e)–(g) processed at an overlapping rate of 50%.

morphology of type I or type II for coatings with or without LSPP were obviously different as indicated in Table 1. Damage morphologies of type I were mainly distributed in the laser fluence of the close-threshold region, and only when the irradiated laser fluence increased above a certain value did damage morphologies of type II begin to appear. The variation tendency of the minimum laser fluence that induced type I damage morphology, which was consistent with that of the LIDTs shown in Figure 4, verified the LSPP process with optimized parameters had a distinct modification of absorbing defects distributed especially within the outermost layer. As indicated by Table 1, the improvement of the minimum laser fluence inducing type II damage morphology was more probably due to the enhancement of mechanical properties as we discussed previously. However, the more definitive synergetic and comprehensive modification process of intrinsic defects, mechanical property and microstructure requires further study in the future. From Figure 4 and Table 1, it was clear that there was a critical shock pressure for the LSPP process, at which the LIDT and the minimum laser fluence inducing type I and type II damage morphologies reached the maximum values of 36.7, 41.4, and 57.5 J/cm^2, respectively. Once the shock pressure is greater than the critical value, the promotion effect of LSPP on the laser-induced damage resistance becomes weakened and could even decrease. Thus, there was a corresponding interval for the LSPP parameters to achieve optimal improvement of the laser-induced damage resistance.

Table 1. The minimum laser fluence inducing type I and type II damage morphologies for coatings without and with LSPP of different parameters.

Sample	Fluence for type I (J/cm^2)	Fluence for type II (J/cm^2)
Without LSPP	14.8	28.3
30%–0.4 J	16.7	30.6
30%–0.5 J	27.1	32.1
30%–0.6 J	31.8	41.4
50%–0.2 J	41.4	57.5
50%–0.3 J	31.5	39.5
50%–0.4 J	12.9	16.9

https://doi.org/10.1017/hpl.2021.4 Published online by Cambridge University Press

3.4. The plasma pressure model

3.4.1. Establishment of the plasma pressure model

Many plasma pressure models[25–28] of LSP have been proposed and researched so far, such as the Fabbro model[25], which is the current most widely recognized model in the application fields of metals and alloys. On account of the experimental fact that the effect of LSPP on dielectric coatings was affected by the coupling of various factors such as the detailed characteristics of absorbing layer and pulse waveform, a plasma pressure equation was established based on a more suitable model proposed by Liu *et al.*[29] to achieve the optimal LSPP parameters and further reveal the improvement mechanism. As shown in the inset in Figure 1(a), during the laser shockwave-forming process, the absorbing layer of the coatings absorbed laser energy and explosively vaporized and evaporated to form a plasma, which formed a three-phase coexistence of gas, liquid, and solid in the treated area. Considering the influence of pulse waveform, the material of confining layer, the peak plasma pressure P' in LSPP process was expressed by the relation[29]

$$P' = \kappa_1\kappa_2 \frac{\sqrt{R^*T}\left(\sqrt{\gamma}+1/\sqrt{\gamma}\right)}{\varepsilon + R^*T\,(1+\gamma/2)} I_0, \tag{1}$$

where κ_1 and κ_2 are influence coefficients of pulse waveform and the confining layer, respectively; R^* is the molar gas constant divided by the molecular molar mass of the substance; γ is the specific heat ratio of the gas; ε is the specific energy of coatings; I_0 is the incident pulse laser intensity, $I_0 = \frac{E}{\tau S}$; E is the laser shock energy, τ is the pulse width, and S is the incident cross-sectional area; T is the temperature of the film surface, $T = \frac{2A\Phi\sqrt{t}}{\sqrt{\pi\lambda\rho c}} + T_0 = \frac{2A\Phi}{\lambda}\sqrt{\frac{\alpha t}{\pi}} + T_0$; α is the thermal diffusivity, $\alpha = \frac{\lambda}{\rho c}$; λ is the thermal conductivity, ρ is the density, and c is the specific heat capacity; T_0 is the initial temperature of the film surface, because $T \gg T_0$, T_0 is generally ignored; A is the absorption rate of the absorbing layer to the laser; Φ is the laser power density, $\Phi = \frac{E}{\tau\pi r^2}$; r is the spot radius; and t is the temperature propagation time.

The peak plasma pressure P' described in Equation (1) is the maximum pressure generated within the duration of a laser pulse. As the experiments involve raster scan processes where pulses are spatially overlapped, test locations are exposed to multiple pressure pulses, even for a single scan. We postulate that these repeated pressure pulses create a cumulative effect in the optical coating, and we therefore calculate the total pressure P for each scan. Based on the experimental fact that the processed laser energy E, spot overlapping rate η, and the number of scans δ could all influence the post-processing effect, I_0 is instead by the more reasonable average laser intensity $En/\tau S^*$, where S^* is the laser shock area, n is the total number of pulses irradiated on the treated area which is equal to the product of n_1 and n_2 (the shot numbers in each line and column), $a = D + D\,(1-\eta)\,(n_1-1)$ and $b = D + D\,(1-\eta)\,(n_2-1)$ are the length and width of the treated area, $\eta = \Delta L/D$, ΔL is the length of the overlap between adjacent spots, and D is the spot diameter. Based on Equation (1) and neglecting the infinitesimal factor $\varepsilon/\sqrt{R^*T}$, the formula of the total pressure P can be obtained as follows:

$$P = \sum_{i=1}^{\delta} \omega_i\kappa_1\kappa_2 \frac{\sqrt{\gamma}+1/\sqrt{\gamma}}{(1+\gamma/2)\sqrt{2AR^*(\alpha t)^{1/2}/\lambda\pi^{3/2}}} \frac{\sqrt{E}nr}{\sqrt{\tau}S^*}, \tag{2}$$

where ω_i is the absorption coefficient of the absorbing layer under the ith scan, which is a variable because the absorbing layer will be consumed after each scan. Notably, when the number of scans $\delta = 1$, $\omega_i = \omega_1 = 1$; when $\delta > 1$, $0 < \omega_\delta < \cdots < \omega_{i+1} < \omega_i < \omega_{i-1} < \cdots < \omega_1 = 1$. Making $\beta = \kappa_1\kappa_2 \frac{\sqrt{\gamma}+1/\sqrt{\gamma}}{(1+\gamma/2)\sqrt{2AR^*(\alpha t)^{1/2}/\lambda\pi^{3/2}}}$, Equation (2) is simplified to

$$P = \sum_{i=1}^{\delta} \omega_i\beta \frac{\sqrt{E}nr}{\sqrt{\tau}S^*}. \tag{3}$$

Table 2. The total pressure of LSPP processes and the obtained LIDT with different overlapping rates and laser energies.

Sample	Total pressure	LIDT (J/cm^2)
30%–0.4 J	0.23β	12.9
30%–0.5 J	0.25β	19.5
30%–0.6 J	0.28β	27.8
50%–0.2 J	0.29β	36.7
50%–0.3 J	0.35β	27.6
50%–0.4 J	0.41β	10.7
30%–0.4 J–2	$0.23\,(1+\omega_2')\beta$	15.9
50%–0.2 J–2	$0.29\,(1+\omega_2'')\beta$	15.9

From the total pressures of LSPP processes under different processing parameters listed in Table 2, the total pressure P was found to increase gradually from 0.23β to 0.41β, as the pulse energy or overlapping rate increased. Although the LIDT increased with increasing P at first, there was an optimum LSPP total pressure 0.29β beyond which the LIDT actually went back down. Therefore, there must be an optimum P of 0.29β, which well confirmed the conclusions speculated from Figures 4 and 5 that there existed a critical pressure of the LSPP process. A considerable promotion effect of LSPP needs reasonable choice of the processing parameters to generate a rational pressure of about 0.28β–0.35β which could achieve the desirable modification of coating on the premise of without breaking through the maximum stress constraint of the coating.

https://doi.org/10.1017/hpl.2021.4 Published online by Cambridge University Press

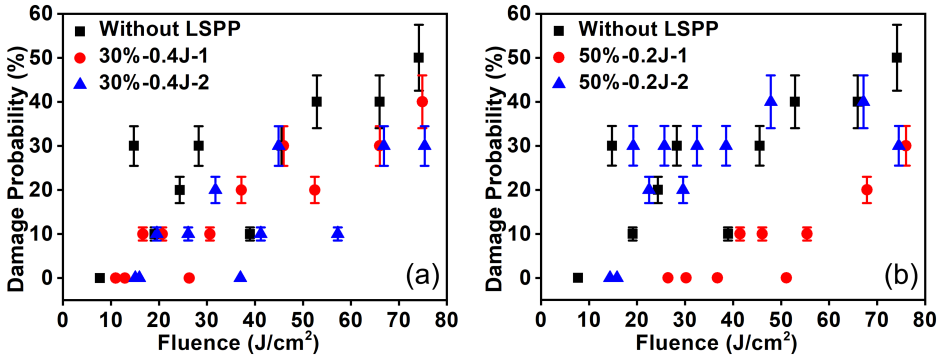

Figure 7. The one-on-one damage probabilities of the 1064 nm HR coatings with or without LSPP under the different numbers of scans (a) at an overlapping rate of 30% and laser energy of 0.4 J and (b) at an overlapping rate of 50% and laser energy of 0.2 J.

3.4.2. Application of the plasma pressure model to two-scan processing

To perfect and further verify the validity of the equation, a preliminary experiment on the effect of the number of scans on total pressure and post-processing effect was also conducted. In our LSPP experiment, macro-damages of coatings occurred once the number of scans was greater than two even with the lowest laser energy 0.2 J; thus we only tried the two scans in some cases herein. As shown in Figure 7, when the number of scans was increased from one to two, the laser-induced damage resistance of coatings post-processed with an overlapping rate of 30% and laser energy of 0.4 J was further improved, yet was weakened with an overlapping rate of 50% and laser energy of 0.2 J. It further suggested the significance of finding the critical total pressure and verified that the number of scans, laser energy, and overlapping rate will all influence the promotion effect of LSPP through changing the total pressures.

The total pressures of the two LSPP processes with the two scans were also calculated using Equation (3) as listed in Table 2. Although the LIDTs were both 15.9 J/cm^2 in these two cases, it was believed that their corresponding total pressures were different and distributed on the two sides of the critical value. By comparing the LIDTs and total pressures listed in Table 2, we infer that $0.23\left(1+\omega_2'\right)\beta$ should be greater than 0.23β and less than 0.25β whereas $0.29\left(1+\omega_2''\right)\beta$ should be greater than 0.35β and less than 0.41β. Thus, the absorption coefficient of the absorbing layer with two scans was found to spread over the range of $0 < \omega_2' < 0.09$ and $0.21 < \omega_2'' < 0.41$. The prediction that $\omega_2' < \omega_2''$ indicated that more absorbing layer was consumed with a higher laser energy of 0.4 J in the first scan, even though the total pressure was relatively low.

4. Conclusion

In summary, the influence of LSPP on the promotion effect of HfO_2/SiO_2 multilayer coatings with different processing parameters has been investigated. The results evidently showed a decrease in damage probability and an increase in LIDT for coatings that had undergone LSPP with appropriate parameters. Although the LSPP process looked as if it had almost no influence on the damage morphology and damage depth, the enhancement of laser damage resistance after LSPP was speculated to be the comprehensive modification of the intrinsic defects and the mechanical properties. Considering the experimental fact that the processed laser energy, spot overlapping rate, and the number of scans all affect the promotion effect of LSPP, a modified equation of total pressure has been established which suggests the existence of a critical total pressure, and given the specific intervals of the total pressure required to achieve a considerable promotion effect of LSPP without breaking through the maximum stress constraint of the coating. The results can help in the interpretation of the mechanism of laser-induced damage and may provide an optional and promising post-processing technique to realize the comprehensive modification of optical coatings.

Acknowledgement

This work was financially supported by the National Natural Science Foundation of China (NSFC) (No. 11704285), the Natural Science Foundation of Zhejiang Province (No. LY20E050027), and the Wenzhou Science and Technology Plan Projects (No. G20170012).

References

1. Z. C. Liu, Y. Zheng, Q. H. Zhang, F. Pan, Y. W. Wei, J. Wang, and Q. Xu, Rev. Sci. Instrum. **88**, 124901 (2017).
2. Y. N. Zhao, T. Wang, D. P. Zhang, S. H. Fan, J. D. Shao, and Z. X. Fan, Appl. Surf. Sci. **239**, 171 (2005).
3. H. B. Li, Y. W. Du, Q. H. Zhang, and Y. W. Wei, J. Appl. Opt. **35**, 902 (2014).
4. K. R. P. Kafka, S. Papernov, and S. G. Demos, Opt. Lett. **43**, 1239 (2018).
5. X. L. Ling, Y. N. Zhao, D. W. Li, J. D. Shao, and Z. X. Fan, Opt. Commun. **283**, 2728 (2010).
6. X. Li, X. F. Liu, Y. A. Zhao, J. D. Shao, and Z. X. Fan, Chin. Opt. Lett. **8**, 598 (2010).

https://doi.org/10.1017/hpl.2021.4 Published online by Cambridge University Press

7. X. F. Liu, D. W. Li, Y. A. Zhao, and X. Li, Appl. Opt. **49**, 1774 (2010).
8. J. F. Sun, A. P. Su, T. M. Wang, W. Y. Chen, and W. Guo, Int. J. Fatigue **119**, 261 (2019).
9. U. Trdan, M. Skarba, and J. Grum, Mater. Charact. **97**, 57 (2014).
10. M. Ducousso, S. Bardy, Y. Rouchausse, T. Bergara, F. Jenson, L. Berthe, L. Videau, and N. Cuvillier, Appl. Phys. Lett. **112**, 111904 (2018).
11. W. F. Zhou, X. D. Ren, Y. Yang, Z. P. Tong, and L. Chen, Mater. Sci. Eng. A **771**, 138603 (2020).
12. Y. Q. Hua, Y. C. Bai, Y. X. Ye, Q. Xue, H. X. Liu, R. F. Chen, and K. M. Chen, Appl. Surf. Sci. **283**, 775 (2013).
13. J. Z. Lu, K. Y. Luo, F. Z. Dai, J. W. Zhong, L. Z. Xu, C. J. Yang, L. Zhang, Q. W. Wang, J. S. Zhong, D. K. Yang, and Y. K. Zhang, Mater. Sci. Eng. A **536**, 57 (2012).
14. A. J. Bischoff, A. Arabi-Hashemi, M. Ehrhardt, P. Lorenz, K. Zimmer, and S. G. Mayr, Appl. Phys. Lett. **108**, 151901 (2016).
15. W. Guo, H. Wang, P. Peng, B. W. Song, H. Q. Zhang, T. W. Shao, H. Huan, H. C. Qiao, G. D. Qu, D. Z. Zhu, and J. F. Yan, Corros. Sci. **170**, 108655 (2020).
16. M. Millot, N. Dubrovinskaia, A. Černok, S. Blaha, L. Dubrovinsky, D. G. Braun, P. M. Celliers, G. W. Collins, J. H. Eggert, and R. Jeanloz, Science **347**, 418 (2015).
17. Y. Shen, S. B. Jester, T. T. Qi, and E. J. Reed, Nat. Mater. **15**, 60 (2016).
18. P. Peyre, R. Fabbro, P. Merrien, and H. P. Lieurade, Mater. Sci. Eng. A **210**, 102 (1996).
19. W. W. Liu, C. Y. Wei, J. B. Wu, Z. K. Yu, H. Cui, K. Yi, and J. D. Shao, Opt. Express **21**, 22476 (2013).
20. P. Yella, P. Venkateswarlu, R. K. Buddu, N. Ravi, K. B. S. Rao, P. P. Kiran, and K. V. Rajulapati, Opt. Laser Technol. **107**, 142 (2018).
21. M.-H. Hong, D. I. Shim, H. H. Cho, and H.-H. Park, Appl. Surf. Sci. **446**, 160 (2018).
22. S. Gürakar and T. Serin, Mater. Sci. Eng. B **251**, 114445 (2019).
23. G. K. Williamson and W. H. Hall, Acta Metall. **1**, 22 (1953).
24. X. F. Liu, Y. A. Zhao, D. W. Li, G. H. Hu, Y. Q. Gao, Z. X. Fan, and J. D. Shao, Appl. Opt. **50**, 4226 (2011).
25. R. Fabbro, J. Fournier, P. Ballard, D. Devaux, and J. Virmont, J. Appl. Phys. **68**, 775 (1990).
26. Z. Y. Duan, H. X. Wu, S. B. Wu, and D. H. Guo, Laser J. **3**, 20 (2000).
27. Y. Qian, R. Q. Xu, J. Lu, and X. W. Ni, Chin. Opt. Lett. **3**, 372 (2005).
28. Y. H. Li, *Theory and Technology of Laser Shock Strengthening* (Science Press, Beijing, 2013).
29. Z. D. Liu, Y. S. Yang, and C. Y. Yu, Aeronaut. Manuf. Technol. **3**, 19 (1993).

https://doi.org/10.1017/hpl.2021.4 Published online by Cambridge University Press